Estimation of Hall Thruster Erosion Using HPHall

IEPC-2005-303

Presented at the 29th International Electric Propulsion Conference, Princeton University, October 31 – November 4, 2005

M. Gamero-Castaño and I. Katz
Jet Propulsion Laboratory, Pasadena, CA , 91108, USA

Abstract: the erosion of the acceleration channel walls of magnetic layer Hall thrusters is one of the mechanism limiting the lifetime of this technology. A good understanding of this phenomenon is important to improve the design of Hall thrusters, predict their operational lifetime, and asses their suitability for space missions. The erosion is caused by the flux of ions impinging on the thruster dielectric walls, and the associated sputtering of the dielectric material. Thus, a good estimate of wall erosion requires accurate knowledge of both the plasma discharge (including ion energies and fluxes to the walls), and the sputtering yield of the dielectric material. In this article we use the HPHall code (J. M. Fife, Ph.D. Thesis, Massachusetts Institute of Technology, 1998) to solve the plasma discharge, together with a sputtering yield model, to simulate the erosion of a SPT-100 Hall thruster. The computed erosion profiles are then compared to erosion measurements available in the literature.

I. Introduction

THE erosion of the acceleration channel walls of Hall thrusters limits the operational life of these engines by exposing the softer elements of its magnetic circuit to the plasma discharge. Therefore a quantitative understanding of the erosion problem, i.e. the determination of the erosion rate and its dependence on the thruster working parameters, will help advancing Hall thruster technology. In particular, there are two applications for which an accurate estimation of the erosion is important: first, it can be used to help designing new engines seeking to maximize lifetime; second, it can be used to estimate the lifetime of an existing engine which must operate in a wide power/mass flow rate range, without the need of an extensive experimental determination of its erosion.

The goal of our research is to create a tool for computing the erosion of the acceleration channels of a Hall thruster. In this article we will use this tool to study a SPT-100 Hall thruster. Two main pieces of information are needed to estimate the erosion: a)the fluxes and energies of the ions hitting the acceleration walls; and b)the sputtering yield for the wall material. We have used HPHall, a numerical code that simulates the plasma discharge of Hall thrusters, to extract the information needed for the ion/projectiles.[1] The treatment of the plasma/wall interactions has been upgraded with the Bohm condition enforcement proposed by Ahedo, and with Ahedo's model for a three-species plasma sheath.[2,3] These modifications are described in sections II.A and II.B. The sputtering yield for $BnSiO_2/Xe^+$, the target/projectile combination (Boron Silicate, $BnSiO_2$, is the ceramic used by the standard SPT-100), has been approximated using Tamamura's model for the sputtering of monoatomic elements,[4] together with experimental data reported by Garnier et al.[5] Section II.C describes our sputtering yield model. In section II.D the SPT-100 plasma discharge is simulated, and erosion rates computed. With this information, the evolution of the channel walls is calculated self consistently. Finally, the numerical erosion results are compared to the experimatal data of Absalamov et al.[6]

II. Discussion

A. Enforcement of the Bohm condition

The original version of HPHall does not impose any constraint on the ions exiting the computational domain to enter a wall boundary (e.g. Bohm velocity condition). Instead, HPHall assumes that the boundary of the

computational domain is the transition between a quiescent plasma (computational domain) and a classical presheath. Both presheath and sheath are solved analytically, and the analytical heat flux and near wall current are used as inputs to the energy and charge conservation electron equations. The classical presheath/sheath solution features, among other things, a zero mean ion velocity at the entrance of the presheath, followed by electrostatic ion acceleration. Eventually, the mean ion velocity reaches the Bohm value at the presheath/sheath transition. Recently, Ahedo has argued that the assumption of an accelerating presheath outside the computational domain is not justified. Two arguments support this idea: first, in typical hall thrusters, the accelerating presheath actually occupies the whole radial extension of the channel; second, in order to be consistent with its sheath model, the HPHall solution should yield a zero ion mean velocity at the domain boundary, which obviously is not observed in the solution (there are ion fluxes to the walls). In view of these shortcomings, Ahedo proposes that the physical boundary condition for HPHall should be that ions must exit the computational domain with Bohm velocity. HPHall should be left to resolve the "presheath", which is indeed part of the computational domain. Unfortunately, the solution generated by HPHall does not fulfill this criterion, and the ions leave the computational domain at velocities well bellow the Bohm value. The disagreement is accentuated when coarser computational grids are used.

To solve this problem, Ahedo modifies the plasma density at the boundary nodes facing a dielectric wall, n_{eQ}, in the following manner:

$$n_{eQ} = \frac{(j_{riQ})_{part}}{e\mathrm{v}_{\mathrm{Bohm}}} \tag{1}$$

where j_{riQ} is the ion flux associated with the boundary node, and $\mathrm{v}_{\mathrm{Bohm}}$ is the Bohm velocity. The original HPHall algorithm computes n_{eQ} by averaging the density of the ions inside the cell of influence of the boundary node. Note that correction (1) consists on using the density value that, multiplied by the Bohm velocity, matches the ion flux yielded by HPHall. Thus, it is the ion Bohm flux, and not the ion Bohm velocity, what is enforced at the computational boundary. This distinction is relevant because the Bohm velocity (which is a function of the electron temperature only) can be compared with the mean ion velocity at the boundaries, to check for the consistency and convergence of the solution. We have implemented Ahedo's algorithm with the following modification:

$$n_{eQ} = \frac{(j_{riQ})_{part}}{e\mathrm{v}_{\mathrm{Bohm}}} \left(1 + \alpha\left(\frac{\mathrm{v}_{riQ}}{\mathrm{v}_{\mathrm{Bohm}}} - 1\right)\right) \tag{2}$$

where α is a free parameter chosen to optimize/speed up the matching between the ion velocity and the Bohm velocity.

Figures 1 and 2 show the average Bohm velocities of the ions entering the inner and outer wall sheaths, obtained with the original HPHall code and when the Bohm condition is enforced. They are associated with a SPT-100 operating at 300 V discharge voltage, and a Xe flow rate of 5.2 mg/sec. Note that the original HPHall solution is far from fulfilling the Bohm velocity condition. Figures 3 and 4 show the electron and ion charge fluxes to the walls. When HPHall imposes charge conservation, it assumes that the fluxes of ions and electrons to the walls balance out. These figures show that these assumption are far from been fulfilled by the original code.

B. Improved sheath model (including secondary electron yield)

The sheath model of HPHall uses the classical Bohm ion velocity at the sheath entrance, which does not take into account the space charge due to secondary electrons; furthermore it does not resolve well the charge saturated regime happening at the high enough electron temperatures associated with a vanishing electric field near the wall. To correct both shortcomings, we have implemented Ahedo's improved sheath model. Ahedo's model considers two different populations of electrons (Maxwellian primaries at constant temperature T_p, and secondary electrons with negligible temperature) and a population of ions inside the sheath; and single ion and electron (again Maxwellian at constant temperature T_e) populations upstream of the sheath entrance. We write bellow a summary of Ahedo's equations that determine the parameters of interests, for the case of negligible ion temperature:

$$m_i \mathrm{v}_{riQ}^2 = T_p \frac{n_{pQ} + n_{sQ}}{n_{pQ} - n_{sQ} T_p / (2e\phi_{QW})} \tag{3}$$

$$\frac{n_{pQ} Exp[-\frac{e\phi_{QW}}{kT_p}]}{4}\sqrt{\frac{8kT_p}{\pi\ m_e}}\ \delta_{eff} = n_{sQ}\sqrt{\frac{2e\phi_{QW}}{m_e}} \tag{4}$$

$$\frac{n_{pQ} Exp[-\frac{e\phi_{QW}}{kT_p}]}{4}\sqrt{\frac{8kT_p}{\pi\ m_e}}\ (1-\delta_{eff}) = n_{iQ}\mathrm{v}_{riQ}^2 \tag{5}$$

$$n_{iQ} = n_{pQ} + n_{sQ} = n_{eQ} \tag{6}$$

$$m_i \mathrm{v}_{riQ}^2 = T_e \tag{7}$$

$$\delta_{eff} = \Gamma[2+B]\ A(kT_p/e)^B \tag{8}$$

where m_i and m_e are the ion and electron masses; e is the electron charge; v_{riQ} is the normal ion velocity at the entrance of the sheath (the subscript Q refers to this location); T_p is the temperature of the primary electrons in the sheath; n_{pQ}, n_{sQ}, and n_{iQ} are primary and secondary electron, and the ion densities at the entrance of the sheath; n_e and T_e are the electron density and temperature in the plasma; ϕ_{QW} is the voltage drop across the sheath (the subscript W refers to the location of the wall); and δ_{eff} is the effective secondary electron yield. Equation (3) is the Bohm condition for the ion velocity at the presheath/sheath transition, from the sheath side; equation (4) is the conservation of secondary electrons in the form of an equality between the fluxes of secondary electrons at the wall and at the entrance of the sheath; equation (5) is a statement of total charge conservation in the sheath including primary and secondary electrons, as well as ions; equation (6) reflects that the electron density at the presheath/sheath transition from the sheath side (n_{pQ}+ n_{sQ}), and the presheath side (n_{eQ}), are equal, and equal to the ion density to preserve charge neutrality in this location; equation (7) is the Bohm ion velocity criterion at the presheath/sheath transition from the presheath side; and equation (8) is a functional form for the effective secondary yield, where Γ is the gamma function and B and A are two fitting parameters than can be obtained from experimental values of the secondary yield of the material of interest. These equations can be solved numerically to obtain n_{pQ}, n_{sQ}, n_{iQ}, v_{riQ}, ϕ_{QW}, and δ_{eff} as a function of the electron temperature, T_e, and plasma density, n_e, at the presheath/sheath transition from the presheath side (these two parameters are values computed by HPHall for the domain boundary).

The above solution is valid until the electric field at the wall becomes zero. This happens when

$$\delta_{eff} = \delta^* \cong 1 - 8.3\sqrt{\frac{m_e}{m_i}} \quad \therefore \quad \frac{e\phi_{QW}}{T_p} = \hat{\phi}_{QW}^* \cong 1.02 \tag{9a, 9b}$$

This point signals the onset of the charged saturated regime, and is associated with a given electron temperature T_e^*. For electron temperatures larger than T_e^*, δ_{eff} remains fixed and equal to δ^*, and n_{pQ}, n_{sQ}, n_{iQ}, v_{riQ}, and ϕ_{QW}, are computed with equations (2), (3), (4), (5) and (7b).

A marginal improvement to Ahedo's model consists of taking into account the energy distribution of the secondary electrons emitted from the wall. Typically, these secondary electrons are emitted with average energies of the order of 2 eV. This value fixes the height of the voltage hump developed near the wall, which turns back the extra flux of secondary electrons and keeps the flux of secondaries into the sheath equal to

$$\frac{n_{pQ} Exp[-\frac{e\phi_{QW}}{kT_p}]}{4}\sqrt{\frac{8kT_p}{\pi\ m_e}}\ \delta^* \tag{10}$$

We have modeled this phenomenon and verified that the effect of the secondary electron's emission energy on the sheath solution is small.

We have used Gascon et al. data to estimate the secondary electron yield function associated with $BNSiO_2$.[7] Using the function $\delta = AT^B$ to fit Gascon's data, we obtain the following least square fitting parameters: A = 0.123, B = 0.528 (T in eV).

Figure 5 shows the voltage drop across the sheath, ϕ_{QW}, versus T_e, computed with both Ahedo's and the original HPHall model. In the case of the Ahedo's model, several secondary electrons energy values have been used. The voltage drop across the sheath is an important contribution to the energy of the sputtering ions, and therefore the erosion rates are very sensitive to sheath voltage drop. Note that the onset of the charge saturated regime occurs around T_e^* = 37 eV for Ahedo's model, while it happens at 29 eV for the original HPHall model. For higher electron temperatures, Ahedo's voltage drop increases and is proportional to T_e, while the HPHall model yields a negligible voltage drop. Figure 6 shows the heat flux to the wall, divided by the plasma density n_{eQ}, computed by both models. The HPHall result overestimates the heat flux for electron temperatures larger than T_e^*. This is due to the exponential dependence of the heat flux on the voltage drop across the sheath: since the voltage drop in the original HPHall model becomes zero beyond T_e^*, primary electrons readily reach the wall (the Boltzmann factor reducing the electron density at the wall is roughly one). On the other hand, Ahedo's model captures correctly the charge saturated regime, the voltage drop across the sheath reaches a minimum at T_e^*, and for larger electron temperatures the heat fluxes are much smaller than in the case of the original HPHall model.

C. Sputtering yield model

Garnier et al. have measured the sputtering yield for $Xe^+ \rightarrow BNSiO_2$ as a function of the incidence angle, and for three projectile energies: 350, 500 and 1000 eV.[8] Unfortunately, these energies are higher than the typical energies of the ions hitting the SPT-100 walls and, for the lack of better data, we will rely on a (sensible) extrapolation of these data to estimate the thruster erosion. Our extrapolation to lower energies is based on a semi empirical law proposed by Yamamura and Tawara for monoatomic solids at normal incidence:

$$Y(E) = F(M_1, M_2, Z_1, Z_2) \times S(\varepsilon(E), M_1, M_2, Z_1, Z_2) \times \left(1 - \sqrt{\frac{E_{th}}{E}}\right)^{2.5} \qquad (11)$$

where M_1 and M_2 are the masses of the projectile and target atom, Z_1 and Z_2 are their atomic numbers, E is the energy of the projectile, and E_{th} is the threshold energy for sputtering. Although Ref(4) gives approximate expressions for the functions F and S, we expect that the complex nature of $BNSiO_2$ will make these approximations unreliable, and we will follow an alternative path to estimate them. First, we expand S in terms of the small parameter ε,

$$S \cong \beta(M_1, M_2, Z_1, Z_2)\sqrt{E} \qquad (12)$$

and regard Fxβ a constant of the Xe+ → $BNSiO_2$ pair. Second, we fit Garnier's data to the following sputtering yield function:

$$Y_V(E) = (\beta_0 + \beta_1\alpha + \beta_2\alpha^2 + \beta_3\alpha^3) \times \sqrt{E} \times \left(1 - \sqrt{\frac{E_{th}}{E}}\right)^{2.5} \qquad (13)$$

where Y_V is the sputtering yield in mm^3/C units, $\beta_0 \ldots \beta_3$ and E_{th} are fitting parameters, and α is the angle of incidence of the projectile with the surface. Using Garnier's data at 350 and 500 eV (the approximation (12) is inaccurate for the case of 1000 eV), we obtain:

$$Y_V(E) = (0.012 - 2.60 \cdot 10^{-4}\alpha + 1.30 \cdot 10^{-5}\alpha^2 - 1.04 \cdot 10^{-7}\alpha^3) \times \sqrt{E} \times \left(1 - \sqrt{\frac{56.9}{E}}\right)^{2.5} \qquad (14)$$

where the angle of incidence and the projectile energy are expressed in degrees and eV. Note that because of the relatively low energy of the SPT-100 ions, a reliable value for the sputtering threshold energy is most important. Although we have not data for $BNSiO_2$ supporting the accuracy of our least square fitting estimate, E_{th} = 56.9 eV,

Chen et al,[9] reports a surface binding energy for BN between 2 and 3 eV, which translates into a threshold energy between 42 and 63 eV. Thus, E_{th} = 56.9 eV is probably a good estimate for the case of $BNSiO_2$.

Figure 7 shows the comparison between Garnier's experimental data and our sputtering yield function (14). Garnier's data are taken from the polynomial fits in his figures. Our sputtering function fits well the data at both energies and for all incidence angles. Figure 8 shows the sputtering yield as a function of the projectile energy, for two incidence angles.

D. Erosion profiles and comparison with erosion measurements

We have tracked the evolution of the SPT 100 channel geometry using the following scheme:

1) The fluxes and energies of the ions hitting the walls are computed as a function of the axial position with HPHall. Typically we run HPHall for 5000 iterations (equal to 250 μs of simulated time, which typically contains four or five oscillations of the discharge current)

2) The erosion rates are calculated with the above information and the sputtering yield function (14).

3) The acceleration channel walls are moved in the direction of their local normal, with a velocity given by the erosion rate. We typically use a Δt of 60 hours to compute the new wall location.

4) The new geometry is imputed to HPHall, and the steps 1) to 4) are repeated until the desired operation time (e.g. 1000 hours) is reached.

We have used a standard SPT 100 operating point to run the calculations: 300 V discharge voltage, and a Xe flow rate of 5.2 mg/sec. The average anode current, thrust and thrusting efficiency computed by HPHall are given in Table I. Note that although the average anode current resembles well the typical value of 4.5 A, the thrust and efficiency are lower than the experimental values, typically 8 mN and 47% respectively. We attribute the lower computed values to inefficient ionization of neutrals in the near plume region, which is not accurately modeled by HPHall. These neutrals result from the neutralization of ions hitting the exit area of the acceleration channel.

The two dimensional magnetic field required by HPHall was constructed with an experimental measurement of the magnetic flux density along the acceleration channel centerline,[10] and the contours of the magnetic stream function given in figure 2, case 2 of Garrigues et al.[11] The magnetic field in the eroded areas of the acceleration channel was computed by extrapolation the stream function contours.

The plots in figure 9 map the plasma density, electron temperature and plasma potential computed by HPHall, at the beginning of operation and after 840 hours. Contours of the magnetic field stream function are given in the potential maps. Note the large curvature of the equipotential lines, which is induced by the enforcement of the Bohm condition. The increased electric field normal to the acceleration channel walls drives a larger ion flux towards the walls.

The acceleration channel profiles at different operation times are plotted in figure 10, together with the profiles measured by Absalamov et al. Note that the upstream point at which the channel begins to erode calculated by HPHall matches reasonable well Absalamov's measurement. The agreement of the shape and depth between the erosion profiles is reasonably good, especially for the outer wall and the earlier operation times. Figure 11 shows the evolution of the radial position at the exit of the channel. We compute a roughly constant speed for the recession of the channel, which does not reproduce the experimental results characterized by a slowing of the recession in time. The poorer agreement at later times can be due to many factors, among which are the lesser accurate magnetic field in the eroded region as the eroded area increases, and the somehow arbitrary downstream boundary condition required by HPHall to integrate the plasma equations (for a lack of better information, we keep it constant throughout the computations).

Tables and Figures.

Table I . Evolution of the thruster discharge current, thrust, and thrusting efficiency

Time (hrs)	0	60	120	180	240	300	360	420	480	540	600	660	720	780	840
$\langle I_A \rangle$(A)	4.43	4.28	4.45	4.45	4.51	4.61	4.60	4.61	4.62	4.64	4.67	4.62	4.46	4.69	4.61
<T>(mN)	7.15	7.03	7.35	7.37	7.51	7.56	7.57	7.52	7.63	7.71	7.76	7.71	7.44	7.81	7.70
η (%)	37.0	37.0	38.9	39.1	40.0	39.7	39.9	39.4	40.5	41.0	41.4	41.2	39.7	41.7	41.2

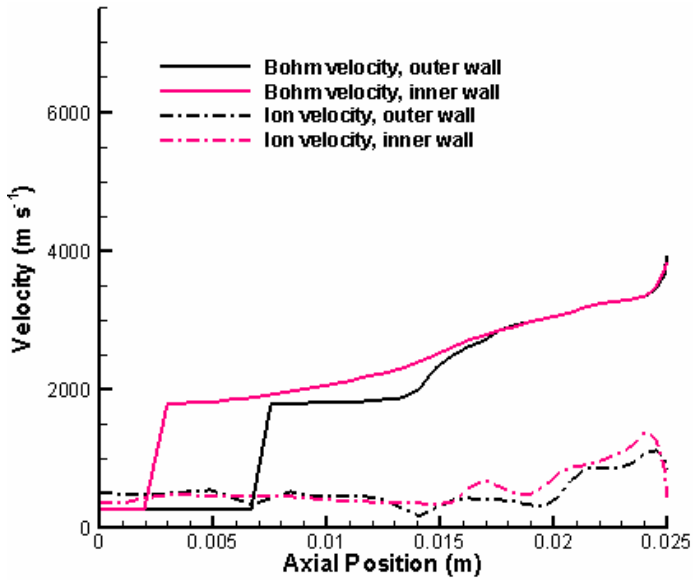

Figure 1. Bohm and average ion velocities at the sheath entrance computed by the original HPHall.

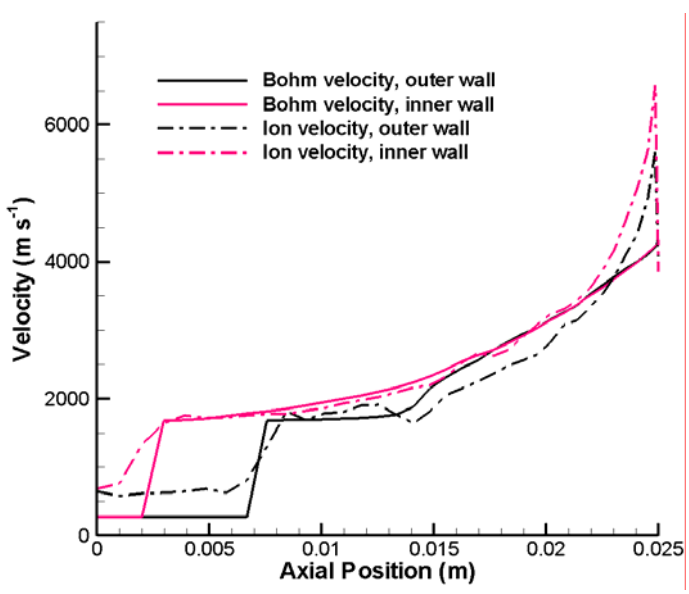

Figure 2. Bohm and average ion velocities at the sheath entrance computed by HPHall when the Bohm velocity condition is enforced.

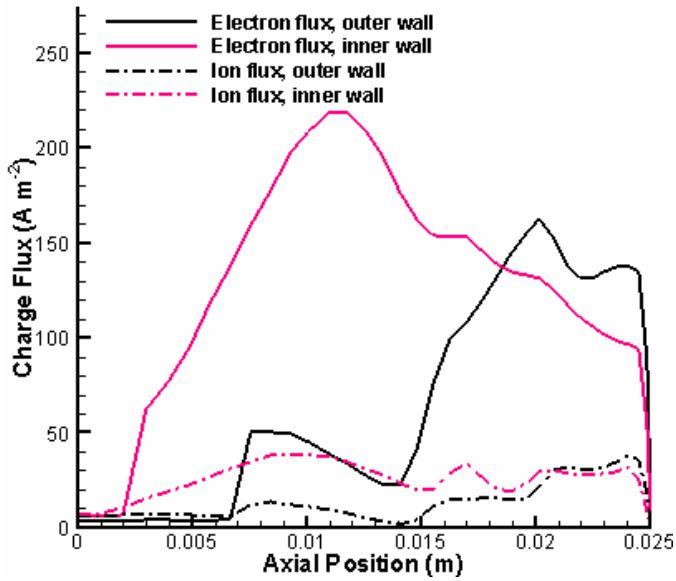

Figure 3. Electron and ion fluxes to the walls computed by the original HPHall.

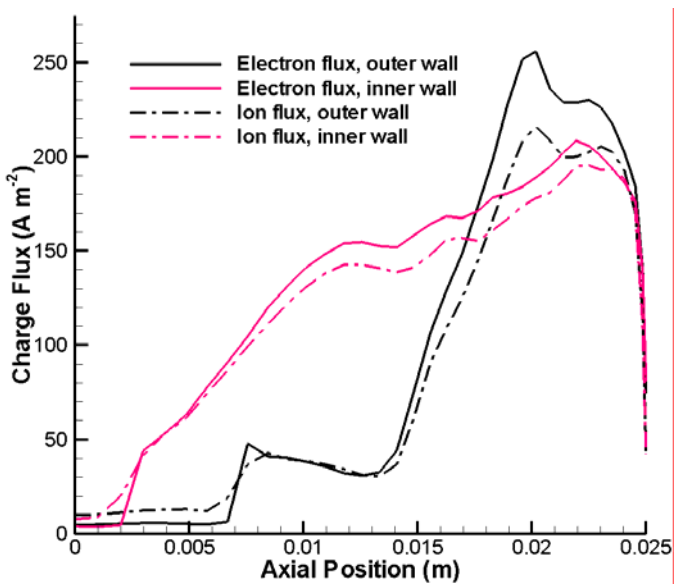

Figure 4. Electron and ion fluxes to the walls computed by HPHall when the Bohm velocity condition is enforced.

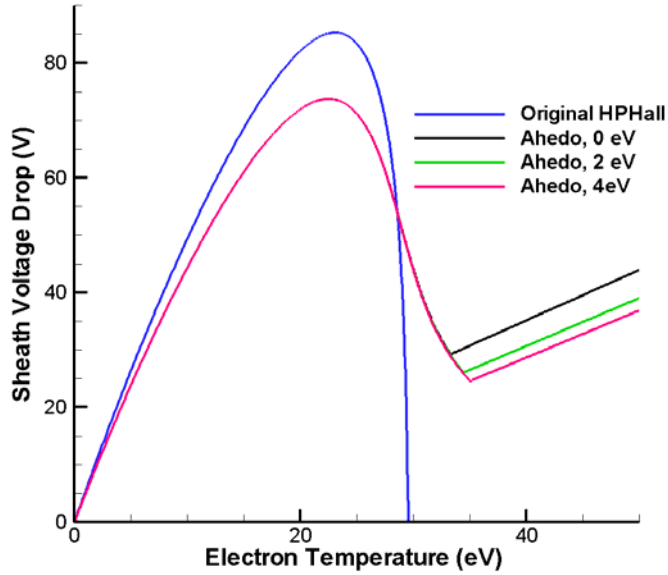

Figure 5. Voltage drops across the plasma sheath used by the original HPHall code, and resulting from Ahedo's model.

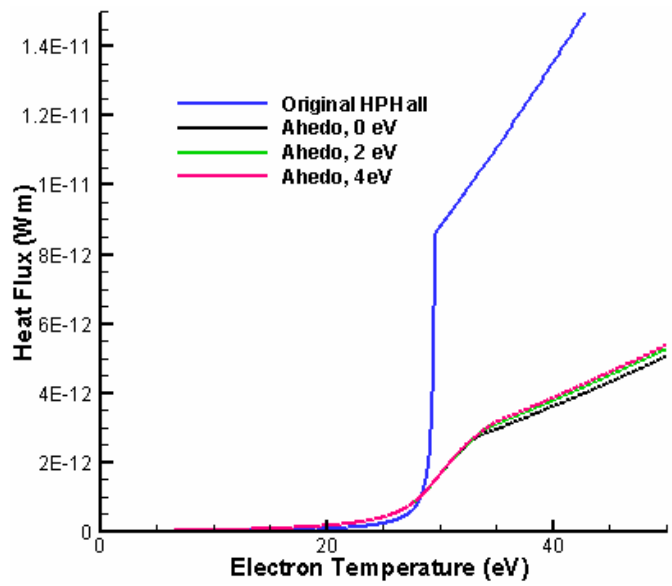

Figure 6. Heat flux across the plasma sheath used by the original HPHall code, and resulting from Ahedo's model.

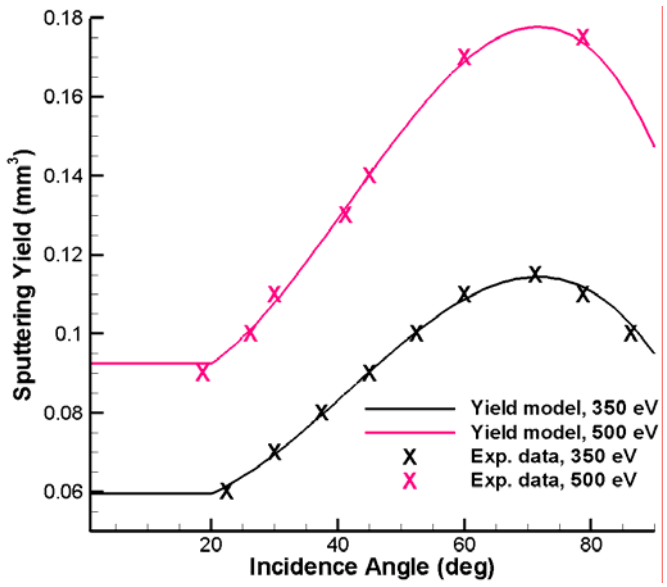

Figure 7. Experimental sputtering yields and sputtering model (equation (14).

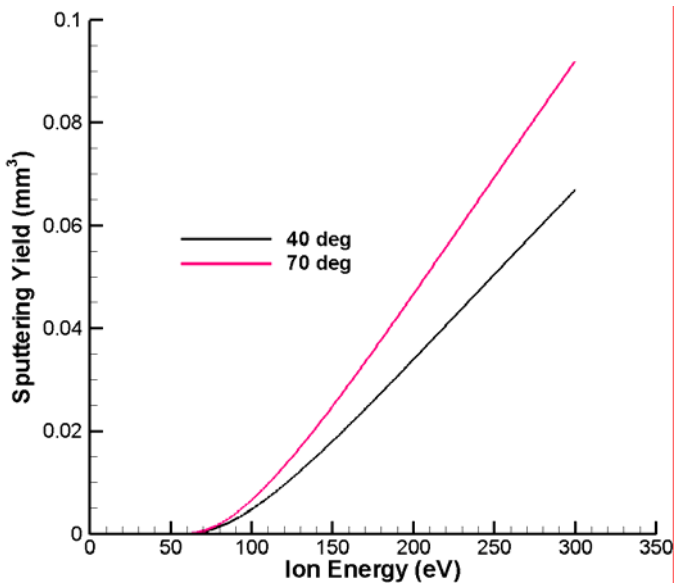

Figure 8. Sputtering yield model for low projectile energies.

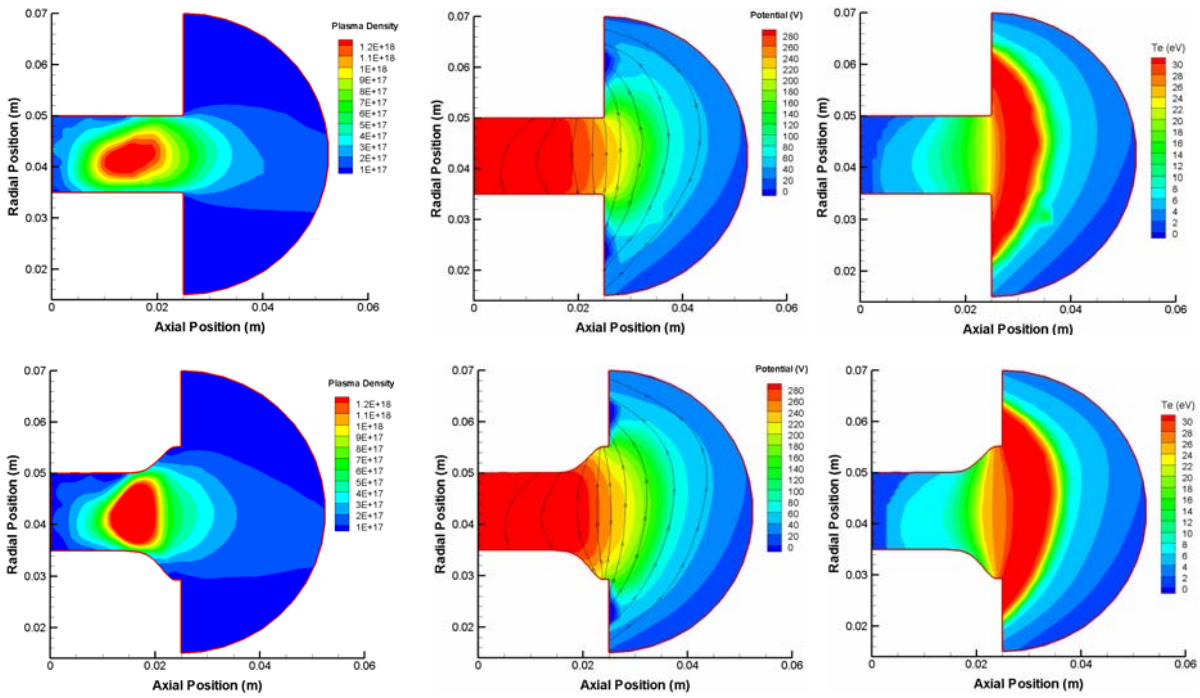

Figure 9. Plasma density, plasma potential, and electron temperature at the beginning of operation and after 840 hours.

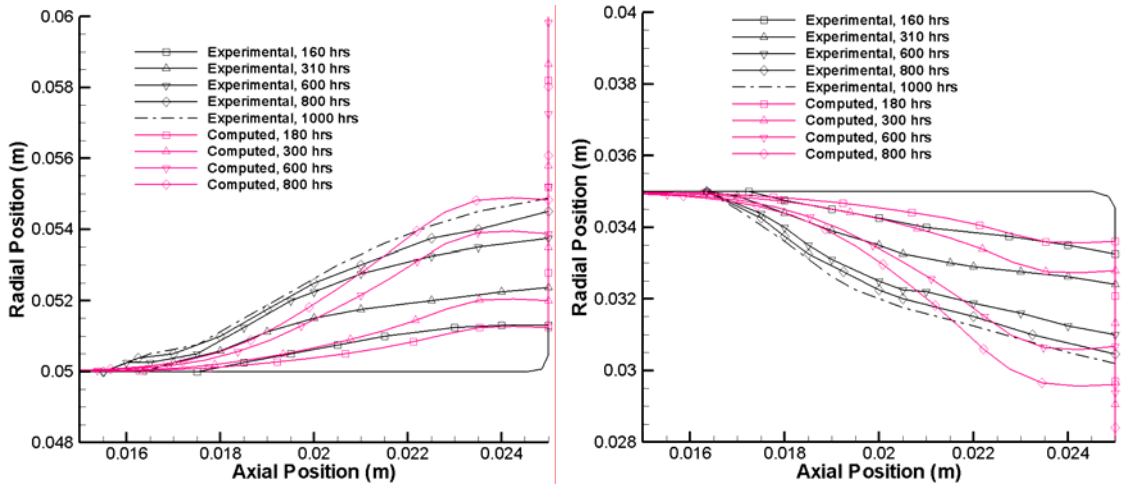

Figure 10. Computed and experimental erosion profiles for the outer and inner acceleration channel walls.

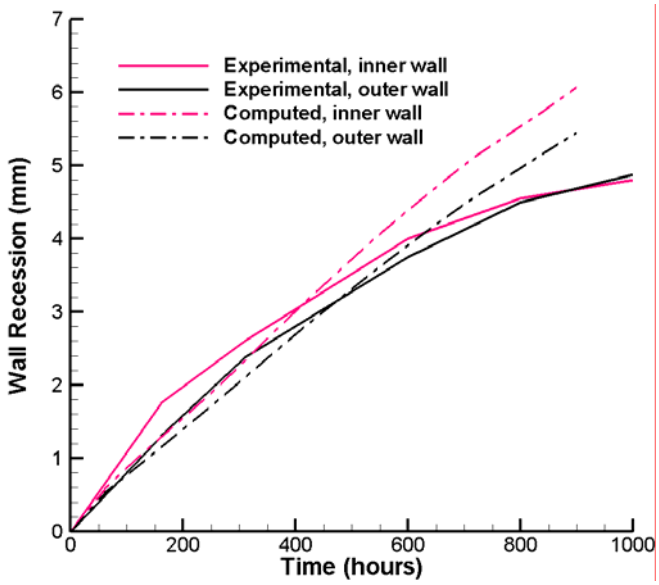

Figure 11. Experimental and calculated evolution of the channel exit.

References

[1] J. M. Fife, "Hybrid-PIC Modeling and Electrostatic Probe Survey of Hall Thrusters", Ph.D. Thesis, Massachusetts Institute of Technology, 1998.

[2] E. Ahedo & F. Parra, "Fulfillment of the Bohm condition on the HPHall fluid-PIC code". AIAA 2004-3955 (2004).

[3] E. Ahedo, "Presheath/sheath model with secondary emission from two parallel walls". Phys. Plasmas, 9,4340-4347 (2002).

[4] Y. Yamamura and H. Tawara, "Energy Dependence of Ion-Induced Sputtering Yields from Monatomic Solids at Normal Incidence", Atomic Data and Nuclear Data Tables, 62, 149-253 (1996).

[5] Y. Garnier, V. Viel, J. F. Roussel, and J. Bernard, "Low-Energy Xenon Ion Sputtering of Ceramics Investigated for Stationary Plasma Thrusters", Journal of Vacuum Science and Technology A, 17,3246-3254 (1999).

[6] S.K. Absalamov et al., " Measurement of Plasma Parameters in the Stationary Plasma Thruster (SPT-100) Plume and its Effect on Spacecraft Components", 28th JPC, AIAA-92-3156 (1992).

[7] N. Gascon, M. Dudeck, and S. Barral, "Wall material effects in stationary plasma thrusters. I. Parametric studies of an SPT-100", Phys. Plasmas, 10, 4123-4136 (2003).

[8] Y. Garnier, V. Viel, J. F. Roussel, and J. Bernard, "Low-Energy Xenon Ion Sputtering of Ceramics Investigated for Stationary Plasma Thrusters", Journal of Vacuum Science and Technology A, 17,3246-3254 (1999).

[9] M. Chen, G. Rohrbach, A. Neuffer, K. Barth, and A. Lunk, "Simulation of Boron Nitride Sputtering Process and Its Comparison with Experimental Data", IEEE Transactions on Plasma Science, 26, 1713-1717 (1998).

[10] We thank Dr. D. Manzella, from NASA Glenn Research Center, for the magnetic flux density data measured along the acceleration channel centerline.

[11] L. Garrigues, G. J. M. Hagelaar, J. Bareilles, C. Boniface, and J. P. Boeuf, "Model study of the influence of the magnetic field configuration on the performance and lifetime of a Hall thruster", Phys. Plasmas, 10, 4886-4892 (2003).